The Computer Simulation of Batch Emulsion Polymerization Reactors Through a Detailed Mathematical Model

K. W. MIN and W. H. RAY,* *Department of Chemical Engineering, State University of New York at Buffalo, Buffalo, New York 14214*

Synopsis

A computational algorithm for the detailed simulation of a batch emulsion polymerization reactor is discussed. The model is applied to the polymerization of methyl methacrylate, and the model predictions are shown to be in good agreement with experimental data. Further computations show the influence of reactor operating conditions on the polymer product and the reactor performance.

INTRODUCTION

Emulsion polymerization in both batch and continuous reactors is a major processing step in the manufacture of polymer products such as paints, inks, coatings, adhesives, high-impact strength copolymers, etc. Current production by emulsion polymerization in the United States is on the order of ten billion pounds per year. In spite of this great economic importance, the detailed mechanistic and quantitative behavior of these reactors is not well understood. For this reason, there is a great deal of interest in developing reliable, predictive mathematical models for emulsion polymerization reactors. Since the early classical work of Harkins, Smith, and Ewart,[1–5] there have been a number of models proposed. Detailed discussions of these models may be found in a number of comprehensive review papers.[6–9]

Most recently,[9] the available models were reviewed and their predictive abilities extensively compared with experimental data. In this same paper, a most comprehensive detailed mathematical model was formulated for emulsion polymerization reactors. This model, which includes all previous models as special cases, consisted of complex multivariate population balance equations coupled to material and energy balances for the reactor. Some brief preliminary computational results from the model have been presented,[10,11] but the full predictive powers of the model have yet to be illustrated, and the computational techniques necessary to simulate the model have yet to be discussed in any detail. It is the purpose of the present paper to show how the complex modeling equations presented in reference 9 may be efficiently solved, to demonstrate how the model parameters may be chosen for a specific polymerization reactor, and to present a detailed comparison of our model predictions with experimental data.

* Present address: Department of Chemical Engineering, University of Wisconsin, Madison, Wisconsin 53706.

Journal of Applied Polymer Science, Vol. 22, 89–112 (1978)
 0021–8995/78/0022–0089$01.00

In the next section, we shall review our mathematical modeling equations for a batch free-radical emulsion polymerization reactor and discuss the model approximations which can readily be made. Following this, we shall outline the numerical procedure which may be used for solving these complex coupled ordinary differential and partial differential–integral equations. Finally, computational results from the model shall be presented for the case of the polymerization of methyl methacrylate and compared with experimental data.

THE MATHEMATICAL MODEL

A very general form of the mathematical modeling equations was presented in reference 9 along with a detailed discussion of the meaning of each part of the model; thus, in this paper, we shall only review the model structure and formulate the necessary equations for treating a batch free-radical polymerization. The model consists of (i) particle size distribution balances, (ii) individual particle balances, (iii) aqueous phase balances, and (iv) general material and energy balances. These balances are coupled and consist of nonlinear ordinary differential equations (ODEs) and population balance equations (PBEs). Although the model structure is very general and can simulate essentially all mechanisms of heterogeneous polymerization which have been proposed, we shall choose a more limited form for demonstration purposes.

The following free-radical kinetic scheme is assumed:
Initiation:

$$I \xrightarrow[k_d]{} 2\mathrm{R}$$

$$\mathrm{R} + \mathrm{M} \xrightarrow[k_i]{} \mathrm{P}_1$$

Propagation:

$$\mathrm{P}_n + \mathrm{M} \xrightarrow[k_p]{} \mathrm{P}_{n+1} \qquad n \geq 1$$

Chain Transfer:

$$\mathrm{P}_n + \mathrm{M} \xrightarrow[k_{fm}]{} \mathrm{P}_1 + \mathrm{M}_n \qquad n \geq 1$$

$$\mathrm{P}_n + \mathrm{Tr} \xrightarrow[k_{ft}]{} \mathrm{P}_1 + \mathrm{M}_n \qquad n \geq 1$$

Termination:

$$\mathrm{P}_n + \mathrm{P}_m \xrightarrow{k_{tc}} \mathrm{M}_{n+m} \qquad n, m \geq 1$$

$$\mathrm{P}_n + \mathrm{P}_m \xrightarrow[k_{td}]{} \mathrm{M}_n + \mathrm{M}_m \qquad n, m \geq 1$$

where the meaning of each of the symbols is given in the Appendix.

The assumptions involved in formulating the model include the following: (i) There is excellent temperature control so that the system is isothermal. (ii) The

polymer particles are homogeneous with no internal structure. (iii) New particles may arise both from micelles and from aqueous phase oligomer precipitation. (iv) Polymer particles are stabilized both by emulsifier and by polymer chain ends on the particle surface. (v) Polymer particle agglomeration is important. (vi) The gel or Trommsdorf effect is present at high conversions. (vii) The monomer concentration in polymer particles depends on particle size, aqueous phase monomer concentration, etc. Under these assumptions, the very general modeling equations presented in references 9 and 12 may be simplified considerably. The various components of the model may be discussed under the following headings.

The Particle Size Distribution Balances

The particle population balance equations include a total particle size distribution balance, $F(V,t)$, which may be written in dimensionless form as

$$\frac{\partial \overline{F}(\overline{V},\overline{t})}{\partial \overline{t}} + \begin{cases} \dfrac{\partial}{\partial \overline{V}}\left[\dfrac{\phi_m}{1-\phi_m}\bar{i}(\overline{V})\,\overline{F}(\overline{V})\right] & \text{for interval I and II} \\ \dfrac{\partial}{\partial \overline{V}}\left[\left(1-\dfrac{d_p}{d_m}\right)\phi_m \bar{i}(\overline{V})\,\overline{F}(\overline{V})\right] & \text{for interval III} \end{cases}$$

$$= \frac{1}{2}C_5 \int_0^{\overline{V}} \exp(-E^*/kT)(\overline{V}-\overline{v})^{-1/3}(\overline{v})^{-1/3}\overline{F}(\overline{V}-\overline{v})\,\overline{F}(\overline{v})\,d\overline{v}$$

$$-C_5\,\overline{F}(\overline{V}) \int_0^{\infty} \exp(-E^*/kT)(\overline{V}\overline{v})^{-1/3}\overline{F}(\overline{v})\,d\overline{v}$$

$$+ C_5 \exp(-E^*/kT)(\overline{V}-\overline{V}_m)^{-1/3}(\overline{V}_m)^{-1/3}\overline{F}(\overline{V}-\overline{V}_m)\,\overline{m}$$

$$- C_5 \exp(-E^*/kT)(\overline{V}\overline{V}_m)^{-1/3}\overline{F}(\overline{V})\,\overline{m}$$

$$+ C_7 H_{\text{eff}m}\overline{m}([\overline{\mathrm{R}}]_w + [\overline{\mathrm{P}}]_w)\bar{\delta}(\overline{V}-\overline{V}_m)$$

$$+ C_{10}[\overline{M}]_w[\overline{P}_{n01}]_w\bar{\delta}(\overline{V}-\overline{V}_0)$$

$$+ C_{11}\left([\overline{\mathrm{P}}]_w{}^2 - \sum_{n=2}^{n_{01}}\sum_{m=1}^{n-1}[\overline{\mathrm{P}}_{n-m}]_w[\overline{\mathrm{P}}_m]_w\right)\bar{\delta}(\overline{V}-\overline{V}_0) \quad (1)$$

where the meaning of the symbols is given in the appendix. It has been found computationally convenient also to consider separately two subsets of the total particle size distribution. The first, $\overline{S}(\overline{V},\overline{t})$, represents explicitly the small particles reappearing in interval III due to the release of emulsifier from the chain end-stabilized particles:

$$\frac{\partial \overline{S}(\overline{V},\overline{t})}{\partial \overline{t}} + \frac{\partial}{\partial \overline{V}}\left[\left(1-\frac{d_p}{d_m}\right)\phi_m(\overline{V})\,\bar{i}(\overline{V})\,\overline{S}(\overline{V})\right]$$

$$= \frac{1}{2}C_5 \int_0^{\overline{V}} \exp(-E^*/kT)(\overline{V}-\overline{v})^{-1/3}(\overline{v})^{-1/3}\,\overline{S}(\overline{V}-\overline{v})\overline{S}(\overline{v})\,d\overline{v}$$

$$- C_5\,\overline{S}(\overline{V}) \int_0^{\infty} \exp(-E^*/kT)(\overline{V}\overline{v})^{-1/3}\overline{F}(\overline{v})\,d\overline{v}$$

$$+ C_5 \exp(-E^*/kT)(\overline{V}-\overline{V}_m)^{-1/3}(\overline{V}_m)^{-1/3}\,\overline{S}(\overline{V}-\overline{V}_m)\,\overline{m}$$

$$- C_5 \exp(-E^*/kT)(\overline{V}\overline{V}_m)^{-1/3}\,\overline{S}(\overline{V})\,\overline{m}$$
$$+ C_7 H_{\text{effm}}\overline{m}([\overline{\text{R}}]_w + [\overline{\text{P}}]_w)\,\bar{\delta}(\overline{V} - \overline{V}_m)$$
$$+ C_{10}[\overline{\text{M}}]_w[\overline{\text{P}}_{n01}]_w\,\bar{\delta}(\overline{V} - \overline{V}_0)$$
$$+ C_{11}\left([\overline{\text{P}}]_w - \sum_{n=2}^{n_{01}}\sum_{m=1}^{n-1}[\overline{\text{P}}_{n-m}]_w[\overline{\text{P}}_m]_w\right)\bar{\delta}(\overline{V} - \overline{V}_0) \quad (2)$$

The second subdistribution, $\overline{U}(\overline{V},\bar{t})$, represents the particles in interval I singly impregnated with growing radicals:

$$\frac{\partial\overline{U}(\overline{V},\bar{t})}{\partial\bar{t}} + \frac{\partial}{\partial\overline{V}}\left[\frac{\phi_m(\overline{V})}{1-\phi_m(\overline{V})}\,\overline{U}(\overline{V})\right]$$
$$= -C_1(\overline{V})^{2/3}([\overline{\text{R}}]_w + [\overline{\text{P}}]_w)\,\overline{U}(\overline{V})$$
$$- C_2\overline{V}[\overline{I}]_p\,\overline{U}(\overline{V})$$
$$- C_3(\overline{V})^{-1/3}\left[\overline{U}(\overline{V})\sum_{n=1}^{n_d} g_n(1,\overline{V})\right]$$
$$- C_5\overline{U}(\overline{V})\int_0^\infty \exp(-E^*/kT)(\overline{V}\overline{v})^{-1/3}\,\overline{F}(\overline{v})\,d\overline{v}$$
$$+ C_5 \exp(-E^*/kT)(\overline{V} - \overline{V}_m)^{-1/3}(\overline{V}_m)^{-1/3}\,\overline{U}(\overline{V} - \overline{V}_m)\,\overline{m}$$
$$- C_5 \exp(-E^*/kT)(\overline{V}\overline{V}_m)^{-1/3}\,\overline{U}(\overline{V})\,\overline{m}$$
$$+ C_7 H_{\text{effm}}\overline{m}([\overline{\text{R}}]_w + [\overline{\text{P}}]_w)\,\delta_{i1}\bar{\delta}(\overline{V} - \overline{V}_m)$$
$$+ C_{10}[\overline{\text{M}}]_w[\overline{\text{P}}_{n01}]_w\delta_{i1}\bar{\delta}(\overline{V} - \overline{V}_0)$$
$$+ C_{11}\left([\overline{\text{P}}]_w{}^2 - \sum_{n=2}^{n_{01}-1}\sum_{m=1}^{n-1}[\overline{\text{P}}_{n-m}]_w[\overline{\text{P}}_m]_w\right)\delta_{i0}\bar{\delta}(\overline{V} - \overline{V}_0) \quad (3)$$

This subdistribution of particles has a single growing radical always and disappears into $\overline{F}(\overline{V},\bar{t})$ after the second radical enters the particle.

The particle size distribution balances also include a radical number distribution, $f_i(V,t)$, which may be written in dimensionless form:

$$\frac{\partial\bar{f}_i(\overline{V},\bar{t})}{\partial\bar{t}} + \begin{cases}\dfrac{\partial}{\partial\overline{V}}\left[\dfrac{\phi_m}{1-\phi_m}\,i(\overline{V})\,\bar{f}_i(\overline{V})\right] & \text{for interval I and II}\\[2ex] \dfrac{\partial}{\partial\overline{V}}\left[\left(1-\dfrac{d_p}{d_m}\right)\phi_m i(\overline{V})\,\bar{f}_i(\overline{V})\right] & \text{for interval III}\end{cases}$$
$$= C_1(\overline{V})^{2/3}([\overline{\text{R}}]_w + [\overline{\text{P}}]_w)\{\bar{f}_{i-1}(\overline{V}) - \bar{f}_i(\overline{V})\}$$
$$+ C_2\,\overline{V}[\overline{\text{I}}]_p\{\bar{f}_{i-2}(\overline{V}) - \bar{f}_i(\overline{V})\}$$
$$+ C_3(\overline{V})^{-1/3}\left\{\bar{f}_{i+1}(\overline{V})\sum_{m=1}^{n_d} g_m(i+1,\overline{V}) - \bar{f}_i(\overline{V})\sum_{m=1}^{n_d} g_m(i,\overline{V})\right\}$$
$$+ C_4\,C_{onc4}(\overline{V})^{-1}\{(i+2)(i+1)\,\bar{f}_{i+2}(\overline{V}) - i(i-1)\,\bar{f}_i(\overline{V})\}$$
$$+ \frac{1}{2}C_5\int_0^{\overline{V}}\sum_{j=0}^{i}\exp(-E^*/kT)(\overline{V} - \overline{v})^{-1/3}(\overline{v})^{-1/3}\,\bar{f}_j(\overline{V} - \overline{v})\,\bar{f}_{i-j}(\overline{v})\,d\overline{v}$$

$$
\begin{aligned}
&- C_5 \bar{f}_i(\overline{V}) \int_0^{\infty} \exp(-E^*/kT)(\overline{V}\overline{v})^{-1/3}\, \overline{F}(\overline{V})\, d\overline{v} \\
&+ C_5 \exp(-E^*/kT)(\overline{V} - \overline{V}_m)^{-1/3}(\overline{V}_m)^{-1/3}\, \bar{f}_i(\overline{V} - \overline{V}_m)\, \overline{m} \\
&- C_5 \exp(-E^*/kT)(\overline{V}\overline{V}_m)^{-1/3}\, \bar{f}_i(\overline{V})\, \overline{m} \\
&+ C_7 H_{\text{eff}m} \overline{m}([\overline{\mathrm{R}}]_w + [\overline{\mathrm{P}}]_w)\delta_{i1}\, \bar{\delta}(\overline{V} - \overline{V}_m) \\
&+ C_{10}[\overline{\mathrm{M}}]_w[\overline{\mathrm{P}}_{n01}]_w \delta_{i1} \bar{\delta}(\overline{V} - \overline{V}_0) \\
&+ C_{11}\left([\overline{\mathrm{P}}]_w{}^2 - \sum_{n=2}^{n_{01}-1} \sum_{m=1}^{n-1} [\overline{\mathrm{P}}_{n-m}]_w[\overline{\mathrm{P}}_m]_w\right) \delta_{i0} \bar{\delta}(\overline{V} - \overline{V}_0) \qquad (4)
\end{aligned}
$$

and in normalized form is

$$
N_i(V,t) = \frac{\bar{f}_i(\overline{V},\bar{t})}{\overline{F}(\overline{V},\bar{t})} \qquad (5)
$$

where

$$
\sum_{i=0}^{\infty} N_i(V,t) = 1. \qquad (6)
$$

The distribution of growing polymer chain lengths, $\hat{f}_n(i,V)$, may be determined from the dimensionless equations

$$
\begin{aligned}
&\frac{\partial \bar{f}_n(i,\overline{V})}{\partial \bar{t}} + \begin{cases} \dfrac{\partial}{\partial \overline{V}}\left[\dfrac{\phi_m}{1-\phi_m} i(\overline{V})\, \bar{f}_n(i,\overline{V})\right] & \text{for interval I and II} \\ \dfrac{\partial}{\partial \overline{V}}\left[\left(1 - \dfrac{d_p}{d_m}\right) \phi_m i(\overline{V})\, \bar{f}_n(i,\overline{V})\right] & \text{for interval III} \end{cases} \\
&= C_1(\overline{V})^{2/3}\{([\overline{\mathrm{R}}]_w + [\overline{\mathrm{P}}]_w)[\bar{f}_n(i-1,\overline{V}) - \bar{f}_n(i,\overline{V})] + ([\overline{\mathrm{R}}]_w \delta_{n1} + [\overline{\mathrm{P}}_n]_w)\, \bar{f}_{i-1}(\overline{V})\} \\
&\quad + C_2 \overline{V}[\overline{\mathrm{I}}]_p\{[\bar{f}_n(i-2,\overline{V}) - \bar{f}_n(i,\overline{V})] + \delta_{n1} 2 \bar{f}_{i-2}(\overline{V})\} \\
&\quad + C_3(\overline{V})^{-1/3} \sum_{m=1}^{n_d} \{g_m(i,\overline{V})\bar{f}_n(i+1,\overline{V}) - g_m(i,\overline{V})\bar{f}_n(i,\overline{V})\} \\
&\quad + C_{61\phi m}(\overline{V})\{\bar{f}_{n-1}(i,\overline{V}) - \bar{f}_n(i,\overline{V})\} \\
&\quad + \{C_{62}\phi_m(\overline{V}) + C_{63}[\overline{\mathrm{T}}_r]_p\}\{i\bar{f}_i(\overline{V})\delta_{n1} - \bar{f}_n(i,\overline{V})\} \\
&\quad + C_4 C_{onc4}(\overline{V})^{-1}\{(i+1)i\bar{f}_n(i+2,\overline{V}) - i(i-1)\bar{f}_n(i,\overline{V})\} \\
&\quad + C_5 \exp(-E^*/kT)\left\{\int_0^{\overline{V}} \sum_{j=0}^{i} (\overline{V} - \overline{v})^{-1/3}(\overline{v})^{-1/3} \bar{f}_n(j,\overline{V} - \overline{v})\bar{f}_{i-j}(\overline{v})\, d\overline{v}\right. \\
&\qquad \left. - \bar{f}_n(i,\overline{V}) \int_0^{\infty} (\overline{V}\overline{v})^{-1/3}\overline{F}(\overline{v})\, d\overline{v}\right\} \\
&\quad + C_5 \exp(-E^*/kT)\{(\overline{V} - \overline{V}_m)^{-1/3}(\overline{V}_m)^{-1/3}\bar{f}_n(i,\overline{V} - \overline{V}_m)\, \overline{m} \\
&\qquad - (\overline{V}\overline{V}_m)^{-1/3}\bar{f}_n(i,\overline{V})\, \overline{m}\} \\
&\quad + C_7 H_{\text{eff}m}\overline{m}([\overline{\mathrm{R}}]_w \delta_{n1} + [\overline{\mathrm{P}}_n]_w)\delta_{i1}\bar{\delta}(\overline{V} - \overline{V}_m) \\
&\quad + C_{10}[\overline{\mathrm{M}}]_w[\overline{\mathrm{P}}_{n01}]_w \delta_{i1}\bar{\delta}(\overline{V} - \overline{V}_0) \\
&\quad + C_{11} \sum_{m=1}^{n-1} [\overline{\mathrm{P}}_{n-m}]_w[\overline{\mathrm{P}}_m]_w \delta_{i0}\bar{\delta}(\overline{V} - \overline{V}_0) H(n - n_{01}) \qquad (7)
\end{aligned}
$$

where a reduced chain length distribution, $g_n(i,V)$, may be defined,

$$g_n(i,V,t) = \bar{f}_n(i,\overline{V},\bar{t})/\bar{f}_i(\overline{V},\bar{t}) \tag{8}$$

which has the property

$$\sum_{n=1}^{\infty} g_n(i,V,t) = i(V) \tag{9}$$

Finally, the distribution of dead polymer chain lengths, $G_n(i,V,t)$, arises from

$$\begin{aligned}
\frac{\partial \overline{G}_n(i,\overline{V})}{\partial \bar{t}} + &\begin{cases} \dfrac{\partial}{\partial \overline{V}}\left[\dfrac{\phi_m}{1-\phi_m} i(\overline{V})\overline{G}_n(i,\overline{V})\right] & \text{for interval I and II} \\ \dfrac{\partial}{\partial \overline{V}}\left[\left(1-\dfrac{d_p}{d_m}\right)\phi_m i(\overline{V})\overline{G}_n(i,\overline{V})\right] & \text{for interval III} \end{cases} \\
&= C_1(\overline{V})^{2/3}([\overline{\mathrm{R}}]_w + [\overline{\mathrm{P}}]_w)\{\overline{G}_n(i-1,\overline{V}) - \overline{G}_n(i,\overline{V})\} \\
&\quad + C_2\overline{V}[\overline{\mathrm{I}}]_p\{\overline{G}_n(i-2,\overline{V}) - \overline{G}_n(i,\overline{V})\} \\
&\quad + C_3(\overline{V})^{-1/3}\sum_{m=1}^{n_d}\{g_m(i+1,\overline{V})\overline{G}_n(i+1,\overline{V}) - g_m(i,\overline{V})\overline{G}_n(i,\overline{V})\} \\
&\quad + \{C_{62}\phi_m + C_{63}[\overline{\mathrm{T}}_r]_p\}\hat{\bar{f}}_n(i,\overline{V}) \\
&\quad + C_4 C_{onc4}(\overline{V})^{-1}\{(i+2)(i+1)\overline{G}_n(i+2,\overline{V}) - i(i-1)\overline{G}_n(i,\overline{V})\} \\
&\quad + C_{403}C_{onc4}(\overline{V})^{-1}\left\{\sum_{m=1}^{n-1} g_m(i+2)g_{n-m}(i+2)\right\}\bar{f}_{i+2}(\overline{V}) \\
&\quad + C_{404}C_{onc4}(\overline{V})^{-1}\{(i+1)g_n(i+2,\overline{V})\bar{f}_{i+2}(\overline{V})\} \\
&\quad + C_5\exp(-E^*/kT)\left\{\frac{1}{2}\int_0^{\overline{V}}\sum_{j=0}^{i}(\overline{V}-\bar{v})^{-1/3}(\bar{v})^{-1/3}\overline{G}_n(j,\overline{V}-\bar{v})\bar{f}_{i-j}(\bar{v})\,d\bar{v}\right. \\
&\qquad \left. - \overline{G}_n(i,\overline{V})\int_0^{\infty}(\overline{V}\bar{v})^{-1/3}\overline{F}(\bar{v})\,d\bar{v}\right\} \\
&\quad + C_5\exp(-E^*/kT)\overline{m}\{(\overline{V}-\overline{V}_m)^{-1/3}(\overline{V}_m)^{-1/3}\overline{G}_n(i,\overline{V}-\overline{V}_m) \\
&\qquad - (\overline{V}\overline{V}_m)^{-1/3}\overline{G}_n(i,\overline{V})\} \\
&\quad + C_{11}\sum_{m=1}^{n-1}[\overline{\mathrm{P}}_{n-m}]_w[\overline{\mathrm{P}}_m]_w\delta_{i0}\bar{\delta}(\overline{V}-\overline{V}_0)H(n-n_{01})
\end{aligned} \tag{10}$$

These complex partial differential–difference-integral population balance equations must be solved numerically, and suitable methods shall be discussed below.

The Remaining Material Balances

The material balances over the individual particles, in the aqueous phase, and in total are essentially as previously described[9] and shall not be rewritten here. It is, however, appropriate to mention how the monomer concentration in the particles was determined. By balancing the free energy of mixing and the surface free energy for a particle, one obtains

$$(1 - \phi_m) + \ln \phi_m + \psi(1 - \phi_m)^2 - \ln\left(\frac{[\overline{M}]_w}{[\overline{M}]_{we}}\right) = -\left(\frac{2\gamma v_m}{RTr_m}\right)\frac{1}{\bar{r}} \quad (11)$$

which may be coupled to a total monomer balance

$$[M_0]_T V_m [\overline{M}]_T - C_{23}\int_0^\infty \phi_m(\overline{V})\overline{V}\overline{F}(\overline{V},\bar{t})\, d\overline{V} - C_{24}V_w[\overline{M}]_w - C_{25}\overline{m}\phi_m(\overline{V}_m) = 0 \quad (12)$$

to yield ϕ_m and $[\overline{M}]_w$ in interval III after the monomer droplets disappear. In the presence of monomer droplets (intervals I and II), $[\overline{M}]_w = [\overline{M}]_{we}$, and only eq. (11) is required.

THE SIMULATION ALGORITHM

In carrying out the numerical solution of the modeling equations, the aqueous phase balances, the particle balances, and the overall material balances are straightforward to handle; they are simply ordinary differential or algebraic equations. In contrast, the population balance equations are coupled multivariate partial differential–difference–integro-differential equations, and their solution represents a very challenging numerical analysis problem. In addition, there are a wide variety of time scales in the reactor, ranging from ~1 sec for free-radical species dynamics to several hours for polymerization to high monomer conversion. Thus, the differential equations are stiff—posing another severe numerical problem. In this section, we shall outline our approach for overcoming these problems in order to produce a computer simulation, but refer the reader to reference 12 for more details.

Solving the Population Balance Equations

There are a large number of possible approaches to the solution of the population balance equations[1–10]; however, unless one chooses extremely carefully, the computing effort could become exorbitant. For our computations, we chose to calculate the leading moments of the distributions and then to represent the explicit differential distributions through a series expansion in the moments. This approach has several advantages. Firstly, the leading moments themselves provide the averages and covariances of the distributions and can be readily compared with experimental data on average particle size, number- and weight-average molecular weights, etc. Secondly, the moments reduce to ordinary differential or algebraic equations which can be readily solved numerically.

The moment equations resulting from the total particle size distribution, $\overline{F}(\overline{V},\bar{t})$, and the two subdistributions, $\overline{S}(\overline{V},\bar{t})$ and $\overline{U}(\overline{V},\bar{t})$, are

$$\frac{d}{d\bar{t}}\overline{\overline{F}}_v[j] = \begin{cases} j\displaystyle\int_0^\infty \left(\frac{\phi_m}{1-\phi_m}\right)\bar{i}(\overline{V})(\overline{V})^{j-1}\overline{F}(\overline{V})\, d\overline{V} & \text{for interval I and II} \\ j\displaystyle\int_0^\infty \left(1 - \frac{d_p}{d_m}\right)\phi_m\bar{i}(\overline{V})(\overline{V})^{j-1}\overline{F}(\overline{V})\, d\overline{V} & \text{for interval III} \end{cases}$$

$$+\frac{1}{2}C_5\exp(-E^*/kT)\sum_{k=0}^{j}\binom{j}{k}\overline{\overline{F}}_v[j-k-1/3]\overline{\overline{F}}_v[k-1/3]$$
$$-C_5\exp(-E^*/kT)\overline{\overline{F}}_v[j-1/3]\overline{\overline{F}}_v[-1/3]$$
$$+C_5\exp(-E^*/kT)\overline{m}\left\{\sum_{k=0}^{j}\binom{j}{k}\overline{\overline{F}}_v[k-1/3](\overline{V}_m)^{j-k-1/3}-\overline{\overline{F}}_v[j-1/3](\overline{V}_m)^{-1/3}\right\}$$
$$+C_7H_{effm}\overline{m}([\overline{R}]_w+[\overline{P}]_w)(\overline{V}_m)^j$$
$$+C_{10}[\overline{M}]_w[\overline{P}_{n01}]_w(\overline{V}_0)^j+C_{11}\left([\overline{P}]_w{}^2-\sum_{n=2}^{n_{01}}\sum_{m=1}^{n-1}[\overline{P}_{n-m}]_w[\overline{P}_m]_w\right)(\overline{V}_0)^j \quad (13)$$

$$\frac{d}{dt}\overline{\overline{S}}_v[j]=j\int_0^\infty\left(1-\frac{d_p}{d_m}\right)\phi_m(\overline{V})\bar{i}(\overline{V})(\overline{V})^{j-1}\overline{S}(\overline{V})\,d\overline{V}$$
$$+\frac{1}{2}C_5\exp(-E^*/kT)\sum_{k=0}^{j}\binom{j}{k}\overline{\overline{S}}_v[j-k-1/3]\overline{\overline{S}}_v[k-1/3]$$
$$-C_5\exp(-E^*/kT)\overline{\overline{S}}_v[j-1/3]\overline{\overline{F}}_v[-1/3]$$
$$+C_5\exp(-E^*/kT)\overline{m}\sum_{k=0}^{j}\overline{\overline{S}}_v[k-1/3](\overline{V}_m\phi_m)^{j-k-1/3}-\overline{\overline{S}}_v[j-1/3](\overline{V}_m\phi_m)^{-1/3}$$
$$+C_7H_{effm}\overline{m}([\overline{R}]_w+[\overline{P}]_w)(\overline{V}_m)^j$$
$$+C_{10}[\overline{M}]_w[\overline{P}_{n01}]_w(\overline{V}_0)^j+C_{11}\left([\overline{P}]_w{}^2-\sum_{n=2}^{n_{01}}\sum_{m=1}^{n-1}[\overline{P}_{n-m}]_w[\overline{P}_m]_w\right)(\overline{V}_0)^j \quad (14)$$

$$\frac{d}{dt}\overline{\overline{U}}_v[j]=j\int_0^\infty\frac{\phi_m(\overline{V})}{1-\phi_m(\overline{V})}(\overline{V})^{j-1}\overline{U}(\overline{V})\,d\overline{V}$$
$$-C_1([\overline{R}]_w+[\overline{P}]_w)\overline{\overline{U}}_v[j+2/3]$$
$$-C_2[\bar{I}]_p\overline{\overline{U}}_v[j+1]$$
$$-C_3\left[\sum_{n=1}^{n_d}g_n(1,\langle\overline{V}\rangle)\right]\overline{\overline{U}}_v[j-1/3]$$
$$-C_5\exp(-E^*/kT)\overline{\overline{U}}_v[j-1/3]\overline{\overline{F}}_v[-1/3]$$
$$+C_5\exp(-E^*/kT)\overline{m}\left\{\sum_{k=0}^{j}\overline{\overline{U}}_v[k-1/3](\overline{V}_m)^{j-k-1/3}-\overline{\overline{U}}_v[j-1/3](\overline{V}_m)^{-1/3}\right\}$$
$$+C_7H_{effm}\overline{m}([\overline{R}]_w+[\overline{P}]_w)(\overline{V}_m)^j$$
$$+C_{10}[\overline{M}]_w[\overline{P}_{n01}]_w(\overline{V}_0)^j \quad (15)$$

The fractional moments which arise in these equations are treated by expanding in terms of integer moments.[12]

In a similar way, the moment equations for the normalized radical number distribution $\overline{N}_i[j](V)$, for the growing polymer chainlength distribution $\hat{\overline{f}}_n[j](i,V)$, and for moments of the dead polymer chain length distribution $\overline{\overline{G}}_{ivn}[0,0,j]$ are formulated.[12]

In solving the moment equations coupled to the material balances for the particles and the aqueous phase, one has only ordinary differential and algebraic equations to solve. In the event that one wishes more detailed information in the form of the explicit differential distributions, one may then expand the

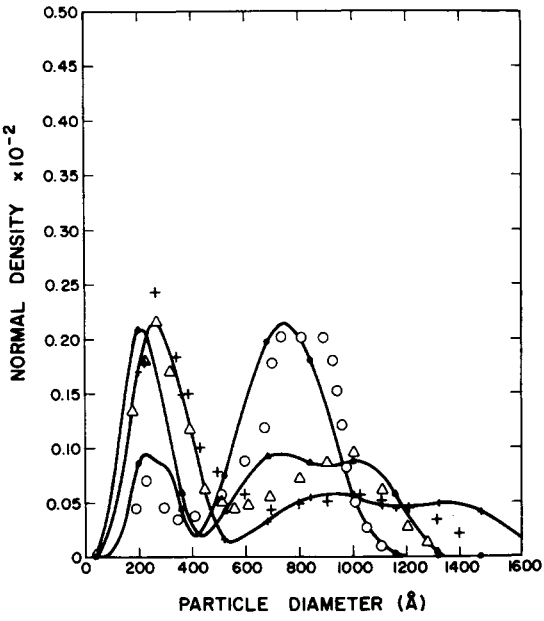

Fig. 1. Particle size distributions for various initial initiator concentrations: (●) $[I_0]_w$ = 18.03 × 10^{-4} g/cc; (▲) $[I_0]_w$ = 3.62 × 10^{-4} g/cc; (+) $[I_0]_w$ = 0.72 × 10^{-4} g/cc; (○△+) Gerrens' experimental data.

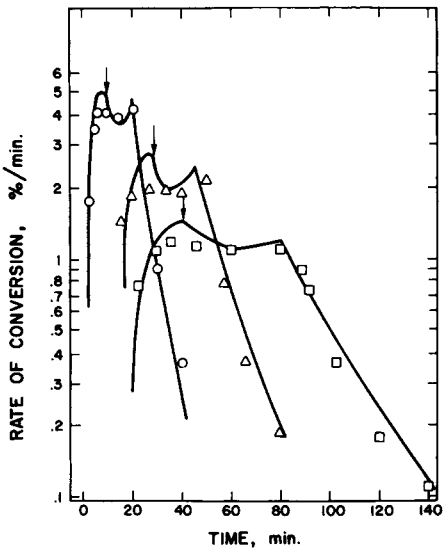

Fig. 2. Evolution of the conversion rate for various initiator concentrations: (○) $[I_0]_w$ = 18.03 × 10^{-4} g/cc; (△) $[I_0]_w$ = 3.61 × 10^{-4} g/cc; (□) $[I_0]_w$ = 0.72 × 10^{-4} g/cc; (↓) starting point of interval III; (—) model predictions.

moments at any specific reaction time in a series expansion in a separate computation. Thus, the computational algorithm can be made quite efficient.

There are several possible expansions one may use to represent the differential distribution. For example, if the distribution is close to a gamma distribution, then expansion in Laguerre polynomials would seem appropriate. On the other

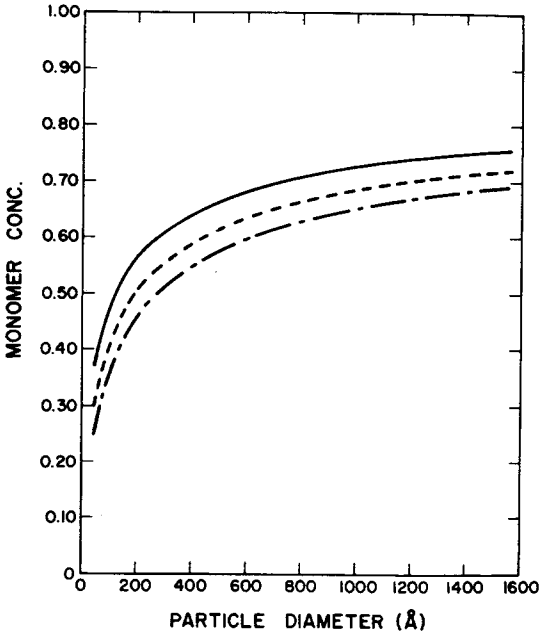

Fig. 3. Monomer concentration in a polymer particle during intervals I and II ($\psi = 0.51$): (—) 5 dynes/cm; (- - -) 8 dynes/cm; (— - —) 11 dynes/cm.

hand, if the distribution resembles a Gaussian distribution, then an expansion in Hermite polynomials would likely be more desirable. A discussion of these and other expansions may be found in reference 12.

The number of moments required for a satisfactory representation of the differential distribution depends on the complexity of the shape. For a unimodal distribution, often only three or four moments are required for a good approximation; however, for a bimodal distribution, 15 or more moments may be required. For this reason, we chose to separate our bimodal particle size distributions into two unimodal distributions, $\bar{S}(\bar{V},\bar{t})$ and $\bar{F}(\bar{V},\bar{t}) - \bar{S}(\bar{V},\bar{t})$, in our computations. In this way, a fewer number of moments are required for an adequate representation.

TABLE I
Comparison of Predictions for Total Number of Particles and Molecular Weights with Experimental Data

Operating conditions		Predictions			Experimental data[13,15,16]	
		Total number of particles $\times 10^{-14}$, #/cc			Total number	
$[I_0]_w \times 10^4$, g/cc	$C_s \times 10^3$, g/cc	At t_{II-III}	At $X_m = 98\%$	$\bar{M}_n \times 10^{-4}$ at $X_m = 98\%$	of particles $\times 10^{-14}$, #/cc	$\bar{M}_\mu \times 10^{-4}$
18.03	5.81	3.40	3.69	4.90	3.32	2.56
3.62	5.81	1.82	3.04	6.18	1.97	5.42
0.72	5.81	0.86	1.80	6.81	1.34	7.03
3.62	11.5	2.14	2.79	6.24	2.28	4.78
3.62	2.91	1.24	1.24	5.81	1.38	5.84
3.62	1.0	0.42	0.42	5.39	0.80	5.60

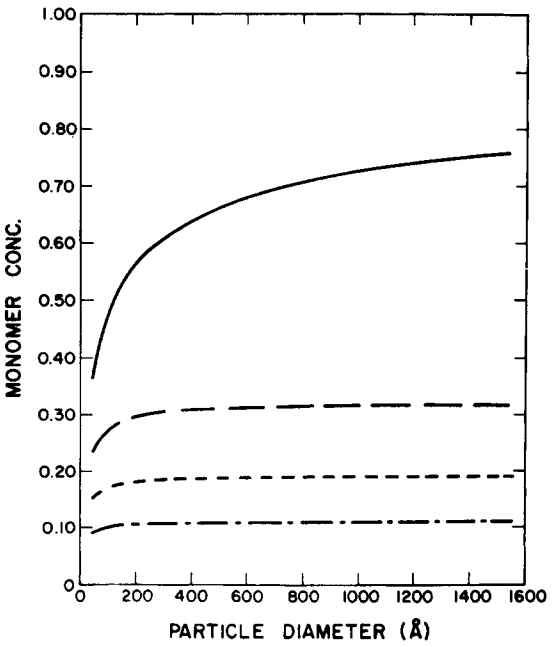

Fig. 4. Monomer concentration in a particle during interval III (ψ = 0.51, γ = 8.0 dynes/cm). Conversion: (—), 29%; (- -) 66.5%; (- - -) 78.6%; (— - —) 87.3%.

The Quasi-Steady-State Approximation

In order to overcome the stiffness in the modeling equations, the quasi-steady-state approximation (QSSA) was made wherever possible. The QSSA was applied to the growing polymer chain length distributions in both the aqueous and particle phase, to the radical number distributions in both phases, and to the dead polymer concentrations in the aqueous phases. The QSSA may be applied to the dead polymer concentration in the aqueous phase because the solubility of polymer in the aqueous phase is so low that the dynamics are extremely fast. This approximation largely relieves the stiffness of the modeling equations, and they may be integrated without undue difficulties.

The Computational Algorithm

The computational algorithm consists of the following steps: (1) Set the initial conditions on all the variables. (2) Calculate the desired number of moments of the distributions $\overline{F}(\overline{V},\overline{t})$, $\overline{U}(\overline{V},\overline{t})$, $\overline{S}(\overline{V},\overline{t})$, $\hat{\overline{f}}_n(i,\overline{V},\overline{t})$, and $\overline{G}_n(i,\overline{V},\overline{t})$ for one time step. (3) Solve for the aqueous-phase concentrations and the free-radical distribution $\overline{f}_i(\overline{V},\overline{t})$, using the quasi-steady-state-approximation. (4) Compute all the remaining material balances. (5) Return to (2) and iterate until the desired reaction time has elapsed. (6) Calculate the explicit differential distributions for $\overline{F}(\overline{V},\overline{t}_j)$, $\overline{S}(\overline{V},\overline{t}_j)$, $\overline{U}(\overline{V},\overline{t}_j)$, etc., based on moment expansions at each time t_j desired.

This algorithm, which is discussed in great detail in reference 12, has been found to be quite efficient. As shall be demonstrated in the next section, it allows a ready comparison of model predictions with experimental data.

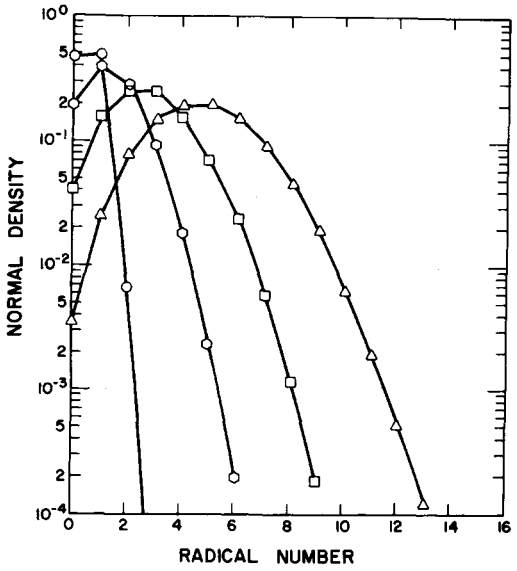

Fig. 5. Radical number distribution in the particle as a function of particle size. Particle diameter in Å: (○) 294; (○) 737; (□) 1003; (△) 1269.

AN EXAMPLE SYSTEM

In order to demonstrate the application of our model and computational algorithm, we have chosen to simulate the batch polymerization of methyl methacrylate (MMA). This monomer has a significant solubility in water, thus allowing aqueous-phase polymerization to play a role. In addition, the gel effect has a strong influence on the polymerization of MMA. Finally, there is a body of data for MMA available with which to compare our model predictions, and these data show that the observed particle size distributions can be quite broad and multimodal. For these reasons, the classical models have been shown[9] to be inadequate for modeling MMA polymerization, and a more detailed model is needed.

A wide variety of model simulations have been generated and are reported in reference 12; however, space limitations only allow a sampling of these to be reported here.

The first task in the modeling of a specific system is to determine the appropriate system parameters. For our study of the MMA system, the kinetic parameters, the dependence of the gel effect on monomer conversion, and the physical properties are all well known and were chosen from the literature. In fact, only two parameters had to be fit to the data. The first of these, H_{effm}, appearing in eqs. (1), (2), (3), and (7) represents the fraction of radicals entering micelles which do not desorb again. This parameter was chosen to be 0.23 for MMA by fitting our predictions for the total number of polymer particles with the data of Gerrens.[13] This is consistent with the value of $H_{effm} \cong 0.1$ used by Harada et al.[14] for the emulsion polymerization of styrene.

The second parameter fitted to the experimental data was E_{ff}, the collision frequency factor for the rate of coalescence of polymer particles. The dependence of the rate of coalescence on surface properties, ionic strength, particle

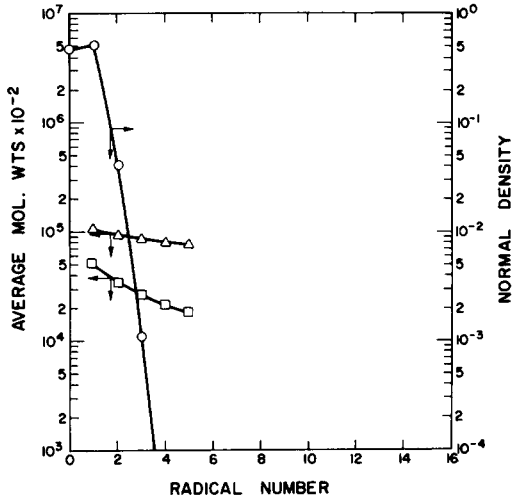

Fig. 6. Molecular weight of growing polymer as a function of radical number for particles of 472-Å diameter (80% conversion): (○) radical number density; (□) number average; (△) weight average.

size, temperature, etc., has been determined theoretically.[9,12] However, the collision frequency factor must be determined empirically. For our model of MMA, the value $E_{ff} = 10$ was chosen based on a fit of Gerrens particle size distribution data.[13]

Having thus selected the appropriate model parameters, it is interesting to compare our model predictions with the experimental data of Gerrens.[13,15,16] In Figure 1, one may see the final particle size distributions compared with the model predictions for a range of initiator concentrations. The total rate of po-

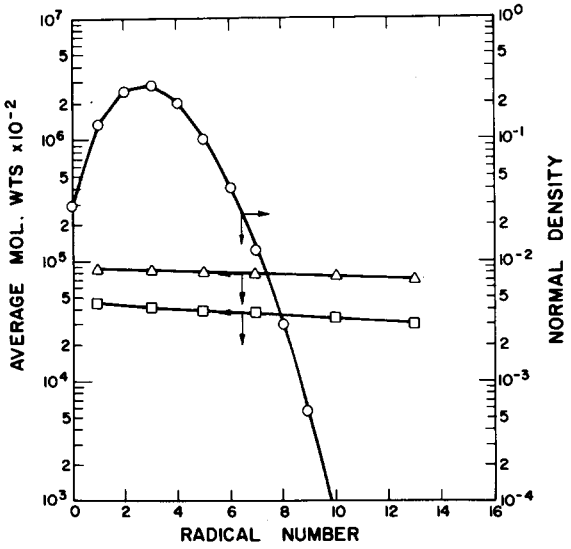

Fig. 7. Molecular weight of growing polymer as a function of radical number for particles of 1182-Å diameter (80% conversion): (○) radical number density; (□) number average; (△) weight average.

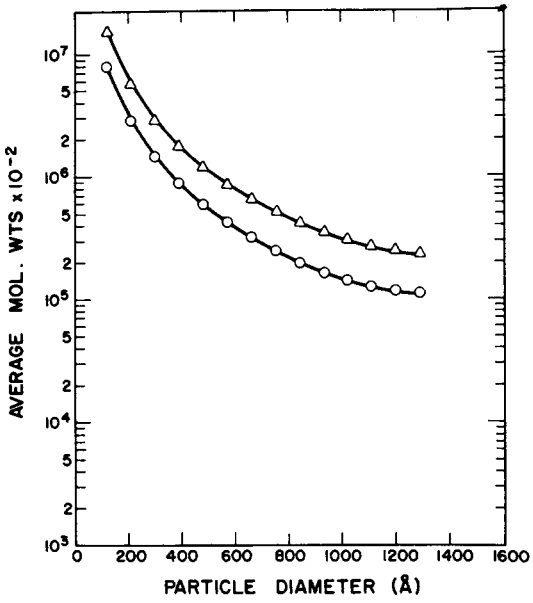

Fig. 8. Molecular weight of growing polymer as a function of particle size at 40% conversion (k_{fm} = 0): (O) number average; (Δ) weight average.

lymerization versus batch time is shown in Figure 2 for the same runs. The agreement of the model with the experimental data is extraordinarily good. The model predictions for molecular weight and total number of polymer particles are compared with the reported data in Table I for a range of initiator and emulsifier concentrations. The number of particles is predicted both at the beginning of interval III and at 98% conversion. The experimentally observed values agree quite well with the predictions. The agreement between predictions

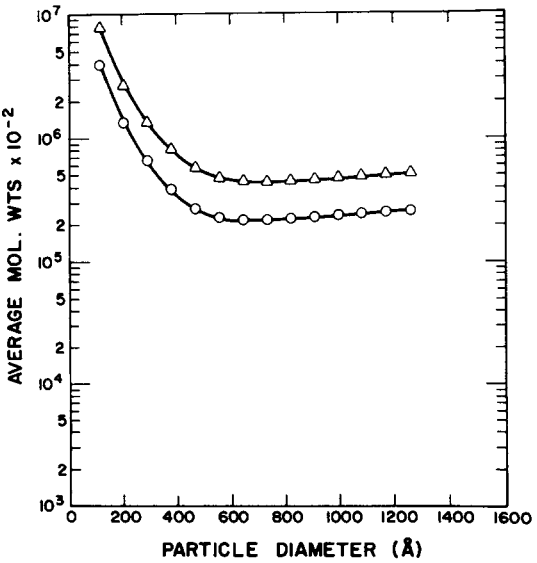

Fig. 9. Molecular weight of growing polymer as a function of particle size at 70% conversion (k_{fm} = 0): (O) number average; (Δ) weight average.

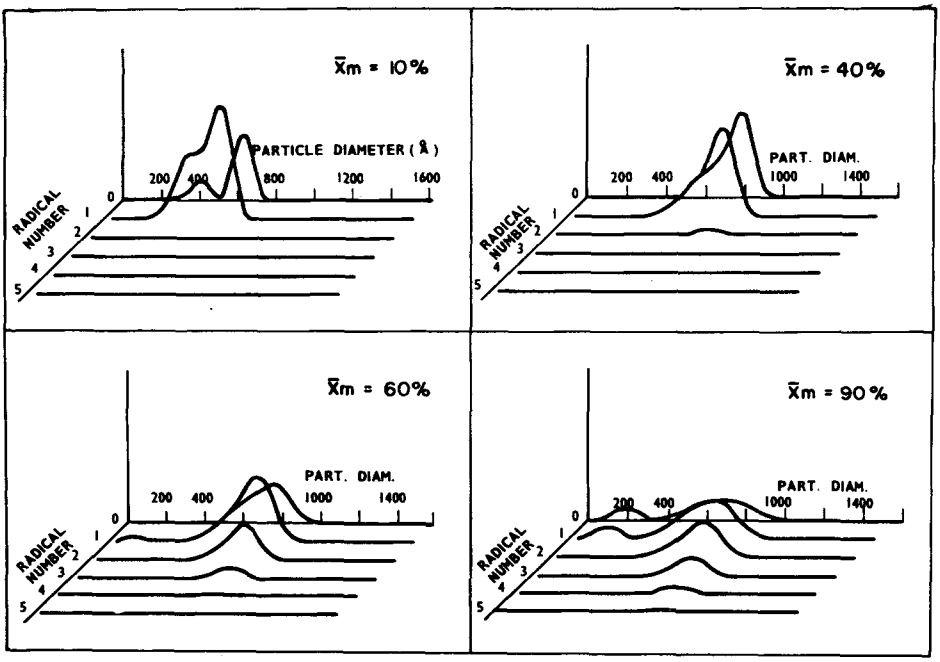

Fig. 10. Evolution of the particle size and free radical distributions.

and measurements for the molecular weight is quite good, except at extremely high emulsifier and initiator concentrations. It is likely that unmodeled chain transfer is causing the experimental molecular weight to be lower than the predictions in these cases.

The ability of our model to predict the observed behavior of a batch MMA emulsion polymerization reactor has been demonstrated for reported data on

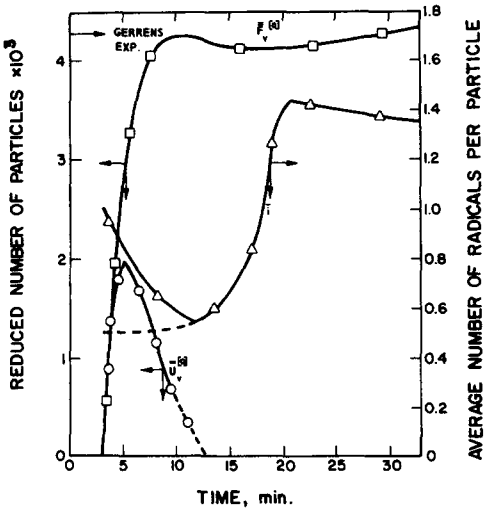

Fig. 11. Evolution of the total number of particles ($\bar{\bar{F}}_v[0]$), the number of singly impregnated particles ($\bar{\bar{U}}_v[0]$), and the average number of radicals per particle: (□) total particles; (○) singly impregnated particles; (△) average number of radicals per article.

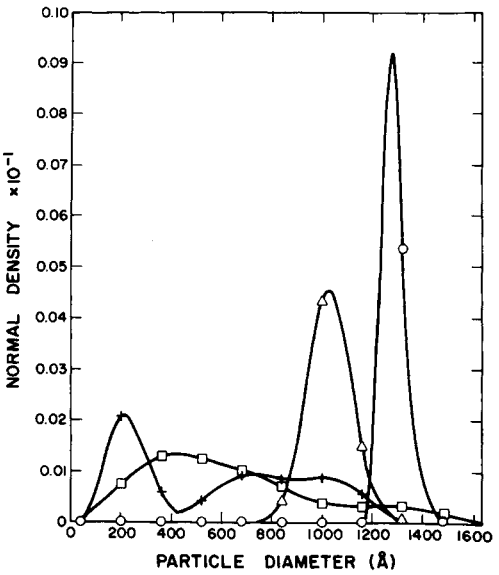

Fig. 12. Particle size distributions for various emulsifier concentrations: (○) $C_s = 1.0 \times 10^{-3}$ g/cc; (△) $C_s = 2.9 \times 10^{-3}$ g/cc; (+) $C_s = 5.8 \times 10^{-3}$ g/cc; (□) $C_s = 11.6 \times 10^{-3}$ g/cc.

conversion, particle size distribution, total particle number, and molecular weight over a range of operating conditions. Now we shall present some predictions from this validated model in order to draw some general conclusions.

The Individual Polymer Particle

The influence of partizle size on the monomer concentration in a single particle may be calculated from eqs. (11) and (12). Typical results, shown in Figures 3 and 4, indicate that in intervals I and II, smaller particles have significantly lower monomer concentrations, but that in interval III, the monomer concentration is nearly independent of particle size and is strongly conversion dependent. Increasing surface tension tends to decrease the particle monomer concentration somewhat.

The distribution of the number of growing radicals in particles of a given size depends strongly on the particle size. Figure 5 shows that very small particles (~300 Å) have principally 0, 1, or 2 radicals while a significant number of larger particles (~1200 Å) have 12 or more radicals per particle.

The molecular weight distribution in polymer particles of a given size depends both on the specific particle size and the number of radicals in the particle. As an illustration, Figure 6 shows that the molecular weight decreases sharply in a small 472-Å particle as the number of growing radicals increases. In contrast, Figure 7 shows that for larger particles, the molecular weight dependence on radical number is much weaker. The influence of the particle size (and the concomitant effects of radical number and monomer concentration) on the molecular weight of the polymer is illustrated in Figures 8 and 9. The molecular weight of polymer formed at relatively low conversions is shown to be strongly dependent on particle size; however, the polymer formed at higher conversions has a molecular weight which is less dependent on particle size.

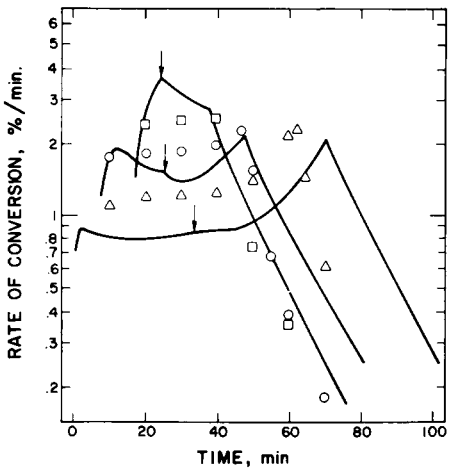

Fig. 13. Evolution of conversion rate for various emulsifier concentrations: (□) $C_s = 11.5 \times 10^{-3}$ g/cc; (○) $C_s = 2.91 \times 10^{-3}$ g/cc; (△) $C_s = 1.0 \times 10^{-3}$ g/cc; (↓) starting point of Interval III; (~) model prediction at each emulsifier concentration.

The higher molecular weight for small particles is due to two effects: (i) The smaller particles have small volumes and a small number of radicals, and chain growth is most strongly influenced by radical entry; in contrast, the larger particles have a large volume and a larger number of radicals, and bulk termination kinetics plays a role in chain growth. (ii) Smaller particles have a lower monomer concentration and a stronger gel effect, thus increasing the molecular weight. The decreased dependence of molecular weight on particle size at high conversions can be explained from Figure 4 where it is seen that the gel effect should be almost particle size independent at high conversions.

Our results[12] also show that the dependence of molecular weight on the particle size depends strongly on the initiator concentration and the amount of chain transfer. For very small initiator concentrations or very high chain transfer rates, the polymer molecular weight is controlled by the chain transfer mechanism and is independent of the particle size.

The Particle Distributions

Having established the influence of operating conditions on the individual polymer particles, we shall now discuss a sampling of particle distributions which arise from the model. Figure 10 shows the evolution of the particle size and free-radical distributions with conversion. At 10% conversion, the particles are fairly small, with essentially 0 or 1 radical per particle. By 40% conversion, the distribution has moved to a larger particle size, and a noticeable fraction of the particles have two radicals. When the conversion reaches 60%, a second small particle peak is beginning due to new free emulsifier in interval III, and some larger particles have three and four radicals. Finally, by 90% conversion, the small particle peak has grown in size and amplitude while the large particles have a rather broad free-radical distribution.

The evolution of the total number of particles and the average number of radicals per particle, $\bar{i}$, is illustrated in Figure 11. Initially, nearly all the particles are singly impregnated [distribution $U(V,t)$], having exactly one radical per

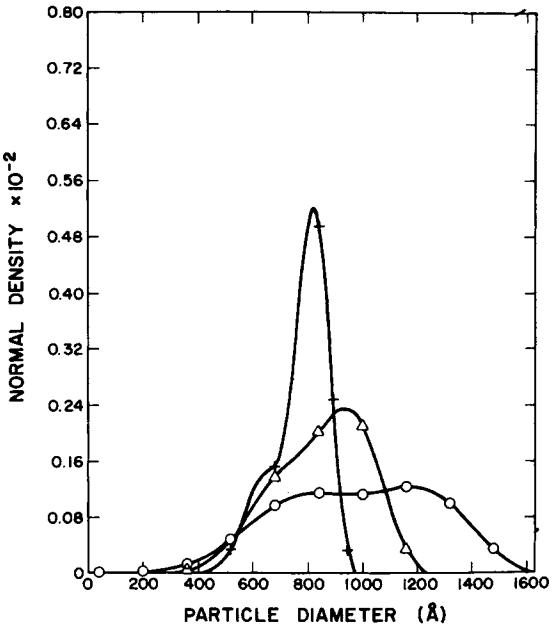

Fig. 14. Particle size distributions at the beginning of interval III with varying ionic strength of the medium: (+) $C_{salt} = 0$; (△) $C_{salt} = 3.0 \times 10^{-5}$ mole/cc; (○) $C_{salt} = 1.0 \times 10^{-4}$ mole/cc.

particle. However, after a short period, the growing particles become multiply impregnated and $\bar{i}$ approaches 0.5, characteristic of small particles. Following this, the particles become larger, and the gel effect becomes important so that $\bar{i}$ increases above 1.0 but begins to level off as the secondary small particles $[S(V,t)]$ are formed at high conversions. Note that the total number of particles remains nearly constant after the initial period and agrees well with Greens' reported value.

The Influence of Operating Conditions

The influence on the reactor behavior of changing initiator concentration has been shown in Figures 1 and 2. In Figure 1, which shows the final particle size distribution as a function of initiator concentration, one may see that a large initiator concentration will cause rapid particle formation so that all the particles are formed almost simultaneously and will grow to a relatively narrow particle size distribution. Alternatively, a small initiator concentration causes slow and protracted particle formation, resulting in a much broader particle size distribution with relatively small numbers of larger particles. The conversion rate history shown in Figure 2 indicates that larger initiator concentrations will lead to higher rates of reaction, as might be expected. The rate of reaction increases sharply as the particles are formed, begins to decrease as the monomer droplets disappear, increases again as the gel effect plays a role, and finally decreases sharply. This latter decrease is likely due to the very low monomer concentration as well as to the propagation constant becoming diffusion limited.

The effect of changing the emulsifier concentration may be seen in Figures 12 and 13. The final particle size distributions as a function of emulsifier con-

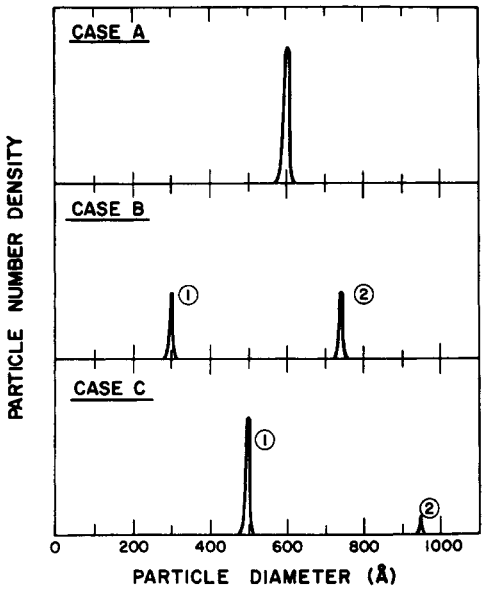

Fig. 15. Comparison of three particle size distributions, each having the same volume average particle diameter.

centration are shown in Figure 12. Very small emulsifier concentrations cause a small number of particles to be formed quickly, and these grow together to form an almost monodisperse size distribution. A very large emulsifier concentration, on the other hand, allows particle formation over a much larger time period and produces a very broad size distribution and a large number of particles. The influence of emulsifier concentration on the predicted conversion rate history is illustrated in Figure 13 and is compared with the experimental data of Gerrens.[13] Although the model is only in fair quantitative agreement with the data, the trends are predicted quite well. As one expects, increasing emulsifier concentration causes the average rate of reaction to increase; however, during the early stages of reaction, the rate is higher for smaller emulsifier concentrations. This is due to the higher rate of propagation in the smaller number of larger particles present at low emulsifier concentrations.

The ionic strength of the polymerizing medium, which is influenced by the concentrations of initiator, emulsifier, chain transfer agents, and other ionic species, seems to have a strong influence on the rate of particle coalescence. This effect is illustrated in Figure 14, where increasing the concentration of an additive salt is predicted to strongly enhance the rate of coalescence, thus broadening the particle size distribution.

CONCLUDING REMARKS

In this paper we have presented some computational results from a very detailed and general model for heterogeneous polymerization reactors. The model was shown to provide very good agreement when compared with experimental data for the batch emulsion polymerization of methyl methacrylate and to allow many mechanistic questions to be explored quantitatively. The computing effort

TABLE II
Influence of Particle Size Distribution on Polymer Molecular Weight and Conversion Rate

	N_1	N_2	d_1, Å	d_2, Å	$\overline{M}_n$	$\overline{M}_w$	Polydispersity	R_p, %/min
				At 20% Conversion				
Case A	1.0	—	600	—	3.77×10^5	7.54×10^5	2.00	5.25
Case B	0.5	0.5	300	740	8.03×10^5	2.416×10^6	3.008	5.06
Case C	0.87	0.13	498	951	4.60×10^5	9.82×10^5	2.134	5.20
				At 80% Conversion				
Case A	1.0	—	600	—	1.40×10^5	2.91×10^5	2.079	3.86
Case B	0.5	0.5	300	740	1.79×10^5	4.371×10^5	2.437	3.94
Case C	0.87	0.13	498	951	1.56×10^5	3.271×10^5	2.102	3.77

required for the simulation of the modeling equations was modest and depended on the degree of detailed information required. As an indication, a simulation of the particle size, radical number, and molecular weight distributions coupled to the reactor material balances over the entire batch time typically required about 12 minutes on the CDC 6400 computer.

There are a number of areas in which work is underway to expand and improve the capabilities of the model. We are working to improve the numerical methods for representing the differential particle distributions as well as developing experimental procedures for better determination of the unknown model parameters for mechanisms such as particle formation, radical desorption, particle coalescence, etc. At the same time, we are applying the model to several example *continuous* emulsion polymerizations to determine how well the model predictions agree with experimental data. Such a continuous reactor model would be of great value in studying experimentally observed reactor oscillations and aid in the solution of continuous reactor control problems.

One of the more interesting questions which such a detailed model can answer for the practitioner is, "what influence does the particle size distribution have on the properties of the polymer produced?" For the MMA system, one may immediately see that the rate of polymerization and molecular weight of the polymer produced depends strongly on the particle size (cf. Figs. 4 and 8) and thus is expected to be influenced by the shape of the particle size distribution. An illustration of this effect may be seen by considering three particle size distributions having the same total number of particles and the same volume-average particle size. Distribution A, shown in Figure 15a, is a unimodal distribution with a narrow peak at 600 Å. Distribution B, depicted in Figure 15b, is bimodal, with 50% of the particles grouped at 300 Å and 50% of the particles grouped at 740 Å. Distribution C, depicted in Figure 15c, is also bimodal, with 50% of the particle volume (87% of the particles) grouped at 498 Å and 50% of the particle volume (13% of the particles) grouped at 951 Å. Calculations were carried out at 20% total conversion (in interval II) and at 80% total conversion (in interval III) to determine the influence of the shape of the particle size distribution. The results, tabulated in Table II, show that in interval III (80% conversion), the molecular weight is slightly influenced by the shape of the particle size distribution. However, in interval II (20% conversion), the particle size distribution has a strong effect on the molecular weight and polydispersity. In both cases, there is a small effect on the rate of polymerization. These results

suggest that in systems without chain transfer control of molecular weight, the molecular weight of the polymer produced can be strongly influenced by the shape of the particle size distribution.

Nomenclature

C_1 = $(k_{mp}/k_p)(d_p/d_m)(N_a)^2[I_0]_w(36\pi)^{1/3}(V_m)^{5/3}$
C_2 = $(k_d/k_p)(d_p/d_m)(N_a)^2[I_0]_w(2f)(V_m)^2$
C_3 = $(k_0/k_p)(d_p/d_m)(N_a)(V_m)^{2/3}$
C_4 = $\{(k_{tc} + k_{td})/2k_p\}(d_p/d_m)$
C_{403} = $(k_{tc}/2k_p)(d_p/d_m)$
C_{404} = $(k_{td}/2k_p)(d_p/d_m)$
C_5 = $(k_c/k_p)(d_p/d_m)(N_a)(m_0)(V_m)^{1/3}$
C_7 = $(k_{mm}/k_p)(d_p/d_m)(N_a)^2[I_0]_w(36\pi)^{1/3}(V_m)^{5/3}$
C_{10} = $(d_p/d_m)(N_a)[I_0]_w{}^2(1/m_0)(V_m)$
C_{11} = $(k_{tc}/2k_p)(d_p/d_m)[I_0]_w{}^2(N_a)(1/m_0)(V_m)$
C_{23} = $(N_a)(m_{\dot{0}})(V_m)$
C_{24} = $(v_m)[I_0]_w$
C_{25} = $(N_a)(m_0)(V_m)$
C_{61} = $(d_p/M_w)(N_a)(V_m)$
C_{62} = $(k_{fm}/k_p)(d_p/M_w)(N_a)(V_m)$
C_{63} = $(k_{ft}/k_p)(d_p/d_m)(N_a)(V_m)[I_0]_w$
C_{onc4} = gel effect coefficient, k_t/k_{t0}
d_m = density of monomer, g/cm^3
d_p = density of polymer, g/cm^3
E^* = activation energy for coalescence, cal/mole
$f_i(V,t)\,dV$ = number of particles containing i radicals in a volume V to $V + dV$ at time t, moles/cm^3 emulsion
$\bar{f}_i(\overline{V},\bar{t})\,d\overline{V}$ = $f_i(V,t)\,dV/m_0$, dimensionless
$\hat{f}_n(i,V,t)\,dV$ = number of radicals of chain length n in the number of particles (per unit volume of emulsion) of size V to $V + dV$ having i radicals, moles/cm^3 emulsion
$\bar{f}_n(i,\overline{V},\bar{t})\,d\overline{V}$ = $\hat{f}_n(i,V,t)\,dV/m_0$, dimensionless
$\bar{f}_n{}^{[j]}(i,\overline{V})\,d\overline{V}$ = jth moment of chain length in dimensionless trivariate growing polymer chain length distribution, $\Sigma_{n=1}^{\infty}(n)^j\bar{f}_n(i,\overline{V})$ $(i,\overline{V})$ $d\overline{V}$
$F(V,t)\,dV$ = number of polymer particles of a volume V to $V + dV$ at time t, moles/cm^3 emulsion
$\overline{F}(\overline{V},\bar{t})\,d\overline{V}$ = $F(V,t)\,dV/m_0$, dimensionless
$\overline{F}_v{}^{[j]}$ = jth moment of dimensionless total particle size distribution, $\int_0^{\infty}(\overline{V})^j\overline{F}(\overline{V})\,d\overline{V}$
$g_n(i,V)$ = number of radicals of chain length n in a particle of size V having i growing radicals, dimensionless
$G_n(i,V,t)\,dV$ = number of dead polymers of chain length n in the number of particles (per unit volume of emulsion) of size V to $V + dV$ having i growing radicals, moles/cm^3 emulsion
$\overline{G}_n(i,\overline{V},\bar{t})\,d\overline{V}$ = $G_n(i,V,t)\,dV/m_0$, dimensionless
$\overline{G}_{ivn}{}^{[0,0,j]}$ = jth moment of chain length n, zeroth moment of radical

number i, and zeroth moment of particle volume V in dimensionless trivariate dead polymer chain length distribution, $\Sigma_{i=0}^{\infty} \int_0^{\infty} \Sigma_{n=0}^{\infty} (n)^j \overline{G}_n(i,\overline{V})\, d\overline{V}$

H_{effm} = fraction of radicals entering micelles which do not desorb again

$\bar{i}(\overline{V})$ = average number of radicals in particles having size $\overline{V}$

I = initiator

$[I_0]_w$ = initial initiator concentration in the aqueous phase

$[\bar{I}]_p$ = $[I]_p/[I_0]_w$ dimensionless initiator concentration in the particle phase

k = Boltzmann constant

k_c = rate constant for particle coalescence = k_c' Eff

k_d = rate constant for initiator decomposition, 1/hr

k_{fm} = rate constant for chain transfer to monomer, cm^3/mole-hr

k_{ft} = rate constant for chain transfer to transfer agent, cm^3/mole-hr

k_i = rate constant for monomer initiation, cm^3/mole-hr

k_p = rate constant for polymer propagation, cm^3/mole-hr

k_{tc} = rate constant for termination by combination, cm^3/mole-hr

k_{mm} = rate constant for radical entry into micelles

k_{td} = rate constant for termination by disproportionation, cm^3/mole-hr

m = number of micelles, moles/cm^3

$\overline{m} = m/m_0$ = dimensionless

m_0 = initial number of micelles

M = monomer

$[\overline{M}]_T$ = $[M]_T/[M_0]_T$, dimensionless

$[M]_w$ = monomer concentration in the aqueous phase, moles/cm^3

$[\overline{M}]_w$ = $[M]_w/[I_0]_w$, dimensionless

$[\overline{M}]_{we}$ = $[M]_w/[I_0]_w$, dimensionless monomer concentration in the aqueous phase in interval I and II

M_n = dead polymer of chain length n

$[M_0]_T$ = initial total monomer concentration in emulsion, moles/cm^3 emulsion

n_{01} = chain length of oligomer in the aqueous phase

$\overline{N}_i^{[j]}(\overline{V})$ = jth moment of normalized radical number distribution, $\Sigma_{i=0}^{\infty} (i)^j N_i(\overline{V})$

$[\overline{P}]_w$ = $[P]_w/[I_0]_w$, dimensionless growing polymer concentration in the aqueous phase

P_n = growing polymer of chain length n

$[\overline{P}_n]_w$ = $[P_n]_w/[I_0]_w$, dimensionless concentration of growing polymer having chain length n in the aqueous phase

$\bar{r} = r/r_m$ = dimensionless radius of a particle

r_m = radius of a micelle, 2.5×10^{-7} cm

R = free radical

$[\overline{R}]_w$ = $[R]_w/[I_0]_w$, dimensionless
$S(V,t)\,dV$ = number of small particles in interval III of a volume V to $V + dV$, moles/cm^3 emulsion
$\overline{S}(\overline{V},\overline{t})\,d\overline{V}$ = $S(V,t)\,dV/m_0$, dimensionless
$\overline{\overline{S}}_v[j]$ = jth moment of dimensionless small particle size distribution, $\int_0^\infty (\overline{V})^j \overline{S}(\overline{V})\,d\overline{V}$
t = time, hr
$\overline{t}$ = $(k_p/N_a)(d_m/d_p)(1/V_m)t$, dimensionless
T_r = chain transfer agent
$[\overline{T}_r]_p$ = $[T_r]_p/[I_0]_w$, dimensionless
$U(V,t)\,dV$ = number of singly impregnated particles of a volume V to $V + dV$, moles/cm^3 emulsion
$\overline{U}(\overline{V},\overline{t})\,d\overline{V}$ = $U(V,t)\,dV/m_0$, dimensionless
$\overline{\overline{U}}_v[j]$ = jth moment of dimensionless singly impregnated particle size distribution, $\int_0^\infty (\overline{V})^j \overline{U}(\overline{V})\,d\overline{V}$
$\overline{v} = v/V_m$ = dimensionless subvariable of particle size
v_m = molal volume of monomer, cm^3/mole
$\overline{V} = V/V_m$ = dimensionless
V_m = volume of a micelle, cm^3
$\overline{V}_m$ = $V_m/V_m = 1$
$\overline{V}_0$ = V_0/V_m, dimensionless volume of precipitating oligomer
V_w = volume fraction of the aqueous phase in emulsion, cm^3/cm^3
γ = surface tension, dynes/cm
δ_{ij} = Kronecker delta function, 1 for $i = j$, 0 for $i \neq j$
$\overline{\delta}(\overline{V} - \overline{V}_m)$ = $\delta(V - V_m)V_m$, dimensionless Dirac delta function, 1 for $\overline{V} = \overline{V}_m$ and 0 for $\overline{V} \neq \overline{V}_m$
$\phi_m(\overline{V})$ = monomer volume fraction in the particle of volume $\overline{V}$
ψ = monomer polymer interaction parameter, dimensionless

The authors are indebted to the National Science Foundation for the support of this research. In addition, they are grateful to Dr. Heinz Gerrens of the BASF, Ludwigshaven, West Germany, for providing many further details about his experimental work.

References

1. W. D. Harkins, *J. Chem. Phys.*, **13**, 381 (1945); *ibid.*, **14**, 47 (1946).
2. W. D. Harkins, *J. Amer. Chem. Soc.*, **69**, 1428 (1947).
3. W. V. Smith, *J. Amer. Chem. Soc.*, **70**, 3695 (1948).
4. W. V. Smith and R. H. Ewart, *J. Chem. Phys.*, **16**, 592 (1948).
5. W. V. Smith, *J. Amer. Chem. Soc.*, **71**, 4077 (1949).
6. H. Gerrens, *Fortschr. Hochpolymer-Forsch.*, **1**, 234 (1959).
7. B. M. E. Van derHoff, in *Solvent Properties of Surfactant Solutions*, K. Shinoda, Ed., Dekker, New York, 1967, Chap. 7.
8. J. W. Vanderhoff, in *Vinyl Polymerization*, Part II, G. E. Ham, Ed., Dekker, New York, 1969, Chap. 1.
9. K. W. Min and W. H. Ray, *J. Macro. Sci.—Rev. Macromol. Chem.*, C11, 177 (1974).
10. K. W. Min and W. H. Ray, *ACS Symposium Series*, **24**, 369 (1976).
11. K. W. Min and W. H. Ray, in *Proc. 4th Int. Symp. Chemical Reaction Engineering*, Heidelberg, April 1976.

12. K. W. Min, Ph.D. dissertation, SUNYAB, 1976, available through University Microfilms, Ann Arbor, Michigan.
13. H. Gerrens, *Dechema Monograph,* **49,** 53 (1964).
14. M. Harada, M. Nomura, H. Kojima, W. Eguchi, and S. Nagata, *J. Appl. Polym. Sci.,* **16,** 811 (1972).
15. H. Gerrens, *Ber. Bunsengesellsch.,* **67,** 741 (1963).
16. H. Gerrens, private communication 1975.

Received September 9, 1976
Revised November 17, 1976